ARTICLE

High Temperature Oxidation Behaviors of Ti-22Al-25Nb Alloy Prepared by Reactive Sintering with Element Powders

Wang Changrui[1,3],　　Wang Yuanxin[2],　　Zhang Kaifeng[2]

[1] Nanjing University of Aeronautics and Astronautics, Nanjing 210016, China; [2] Harbin Institute of Technology, Harbin 150001, China; [3] The 14th Research Institute of China Electronics Technology Group Corporation, Nanjing 210039, China

Abstract: Ti-22Al-25Nb is a high-temperature structural material whose oxidation resistance will be important for its further developments and applications. In this study, the oxidation behaviors of sintered Ti-22Al-25Nb alloy which was prepared by reactive sintering with element powders were investigated in the temperature range of 650~950 °C in static air. The maxima of the mass gains at different temperatures (650, 750, 850, 950 °C) were 0.15, 0.41, 1.68 and 6.9 mg·cm^{-2}, respectively. The Ti-22Al-25Nb sintered alloy exhibited a good oxidation resistance, especially below 750 °C (with breakaway oxidation occurring at 950 °C). According to the oxidation kinetics analyses, the oxidation behaviors approximately followed the parabolic law below 750 °C. Whereas, with temperatures rising above 850 °C, the oxidation behaviors fitted the linear law. Oxidation kinetics were discussed with regard to the influence of the Nb alloying element. Based on the observations and analyses of the oxidation morphologies and phases, it was proven that the oxidation resistance of the O phase (orthorhombic Ti$_2$AlNb) was superior to those of others. The reason for this phenomenon was the difference of Nb content in different phases could result in a difference of oxidation resistance.

Key words: Ti-22Al-25Nb sintered alloy; orthorhombic phase; high-temperature oxidation; oxidation mechanism

Ti$_2$AlNb (O-Ti$_2$AlNb, orthorhombic structure Ti$_2$AlNb) alloys have high specific strength, high fracture toughness, and high creep resistance[1-5]. Thus, Ti$_2$AlNb alloys were developed as a potential candidate for new high temperature structural materials since being found by D. Banerjee[6]. Ti$_2$AlNb have been expected to be applied in the temperature range of 600~800 °C. Thus, their anti-oxide performance was a key factor for their applications at elevated temperatures due to the increasing requirements of higher temperature for Ti$_2$AlNb alloys. In addition, many traditional crafts and techniques were conducted at higher temperatures in order to increase efficiency; this would put forward higher demands for Ti$_2$AlNb alloy applications[7,8]. Li studied electron beam-welded Ti$_2$AlNb alloy joints for applications in aeronautics and astronautics[9]. The dynamic chip formation mechanisms of Ti$_2$AlNb intermetallic alloy were also explored[10]. The deformation behaviors of Ti$_2$AlNb were also investigated at elevated temperatures[11].

Moreover, high-temperature oxidation could lead to a decrease in performance and a shortening of work life for parts or equipment. Therefore, in order to evaluate the thermal stability of the alloys for high temperature applications, it is important to study the high-temperature oxidation behaviors of Ti$_2$AlNb alloys, to analyze their oxidation mechanism, and to assess their oxidation resistance in the used temperature range. Zhang pointed out that the oxidation behavior of Ti$_2$AlNb alloys was improved due to the formation of Al$_2$O$_3$ or NiCr$_2$O$_4$ film[12]. Chen have pointed out that the formation of Al$_2$O$_3$ prevented the oxidation of Ti$_2$AlNb, while the formation of AlNbO$_4$ accelerated oxidation[13]. Leyens studied the oxidation behaviors and hardness changes of Ti$_2$AlNb at high temperatures[14]. However, the high temperature oxidation behaviors of Ti-22Al-25Nb were seldom studied.

Thus, in this work, the isothermal oxidation testing of the reaction-sintered alloy Ti-22Al-25Nb in the Ti$_2$AlNb-based

alloy in the target applied temperature range of 650 to 950 °C was carried out. The oxidation process was observed, the oxidation law was summarized, the oxidation rate was measured and the oxidation mechanism was analyzed. Therefore, the advantages and disadvantages of its oxidation resistance could be pinpointed, which provided a theoretical basis and reference for the optimization design of the composition and properties of the sintered Ti-22Al-25Nb alloy.

1 Experiment

The Ti-22Al-25Nb alloy was prepared by reactive sintering and hot pressing with element powders, which were composed of B2, O and Ti₃Al phases, as shown in Fig. 1. The samples with dimensions of 9 mm× 9 mm× 5 mm, were cut from Ti-22Al-25Nb alloy with electrical discharge machining. The samples were ground with 1200# SiC abrasive paper and then polished and cleaned using acetone and ethanol. The superficial area was measured and the samples were weighted before oxidizing. A high purity alumina crucible was used as a container for holding samples. The crucible was calcined and cleaned at a high temperature before being used, and then weighed accurately. The oxidation tests were performed in air at 650, 750, 850 and 950 °C, holding for 12, 24, 36, 48 and 72 h. In order to ensure uniform oxidation, the samples were slanted in the crucible, which caused the surface of the sample to be fully in contact with the air. Δm (mass gain) was also calculated after oxidation tests. The k_p (oxidation rate constant) was obtained by the means of curve fitting in Origin 8.0. The samples were weighted by electronic balance (The weighing accuracy is 0.01 mg). The oxidation phases of the oxidation scales were identified by XRD X-ray diffraction and EDS (energy dispersive X-ray spectrometry) (on SEM). The surface morphologies and cross-sectional morphologies of the oxidized samples were observed by SEM (scanning electron microscopy).

2 Results and Discussion

2.1 XRD phase analyses of oxide films of the Ti-22Al-25Nb sintered alloy
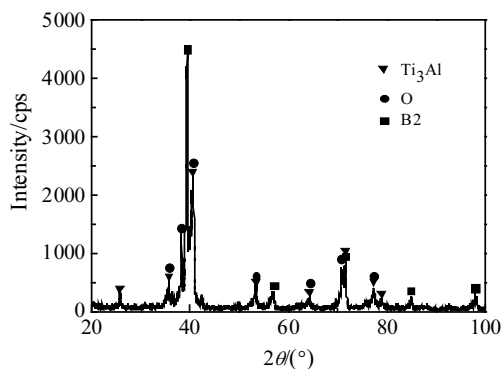
Fig.1   XRD pattern of alloy sintered at 630 °C, 20 MPa, 1 h; 1250 °C, 30 MPa, 2 h

Fig.2 shows the XRD patterns of the surface of samples oxidized for 72 h at 650, 750, 850 and 950 °C. As can be seen in Fig. 2a, the mixed oxides consisted of TiO₂, Al₂O₃ and Nb₆O. Nevertheless, the O phase was still detected. This revealed that the oxidation reaction was not obvious, and the oxidation scale should be thin. Nb would be prone to forming a metastable phase at the low temperature stage for Nb₆O oxide, having lower activation energy. While the temperature increased, as shown in Fig. 2b, Nb oxide (metastable phase) continued to be oxidized. The metastable Nb₆O transformed into NbO and Nb₂O₅. The formation of AlNbO₄ revealed that fast-growing Nb₂O₅ could react with Al₂O₃. However, O-Ti₂AlNb was still detected. This also suggested that the oxidation resistance of the O phase was superior to that of others.

XRD analyses in Fig. 2c and Fig. 2d indicated that the oxidation scales mainly consisted of TiO₂, AlNbO₄, Nb₂O₅ and a small amount of Al₂O₃ at 850 and 950 °C. There was no difference between the two in their composition of oxide when the temperature rose above 850 °C. This indicated that the oxidation reaction had a tendency to be stable. Comparing XRD analyses of the oxidized scale in Fig. 2a and Fig. 2b, it was obvious that the unoxidized O phases were not found. This proved that the oxide films had enough thickness to cover the surface of the sintered alloy at higher temperatures. Furthermore, all metastable Nb oxides of Nb₆O and NbO continued to transform into the stable Nb₂O₅. Meanwhile, Nb₂O₅ reacted with Al₂O₃, which caused Al₂O₃ to be consumed gradually. This also resulted in a decrease of Al₂O₃ content, as shown in Fig. 2c and Fig. 2d. In conclusion, the XRD analyses showed that the oxides also mainly consisted of TiO₂, which was verified roughly from the peak of the XRD analyses. Similarly, Li et al. [15] studied the oxidation behavior of Ti-22Al-26Nb alloy at 750 °C. They found that the oxide composites were mainly composed of TiO₂ and Nb₂O₅ (AlNbO₄) while holding for 200 h.

2.2 SEM observation of the surface morphologies for oxidized specimens

Fig.3 shows the BSE and SE images of the microstructure of the sintered Ti-22Al-25Nb alloy. The Ti-22Al-25Nb alloy was prepared by reactive sintering and hot pressing with element powders. As can be seen in Fig. 3a, the Ti-22Al-25Nb sintered alloy was mainly composed of O, B₂ and a little Ti₃Al phases (the light color marks the B₂ phase, the grey indicates the O phase, and the dark grey denotes the Ti₃Al phase). In addition, it can be observed in Fig. 3b that a large-grained microstructure existed in the sintered alloy, and the finer equiaxed Ti₃Al was prone to occurring in grain boundary.

Fig.4 shows the surface morphologies of oxidation films at different temperatures. As can be seen from it, the growth of oxidation films was obvious with the increasing temperature.
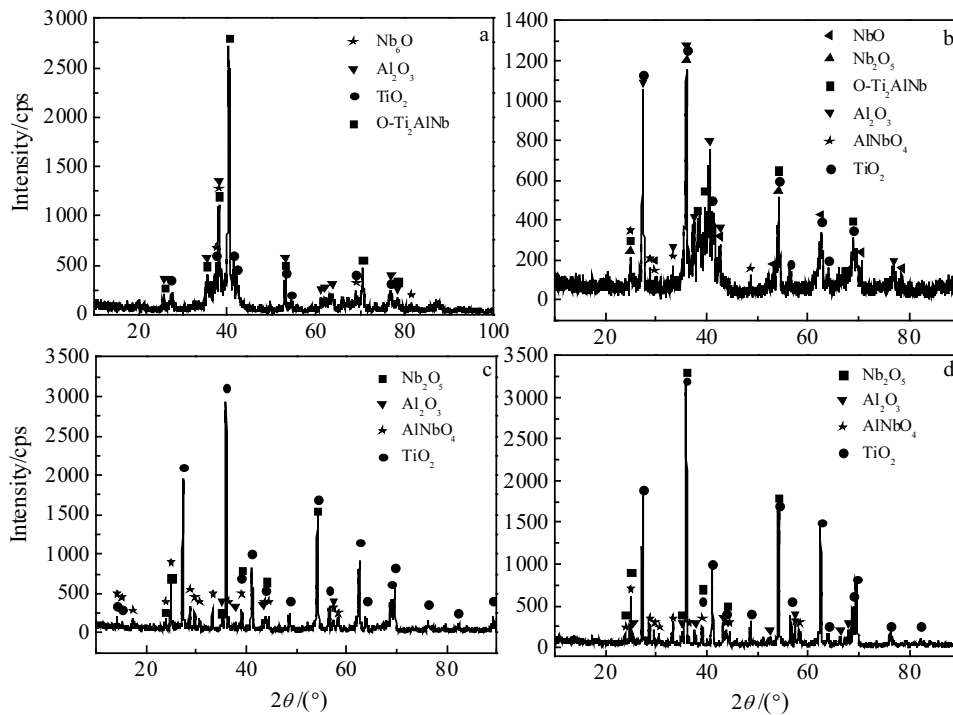
Fig.2   XRD patterns of the surface of the samples oxidized for 72 h at different temperatures: (a) 650 °C, (b) 750 °C, (c) 850 °C, and (d) 950 °C
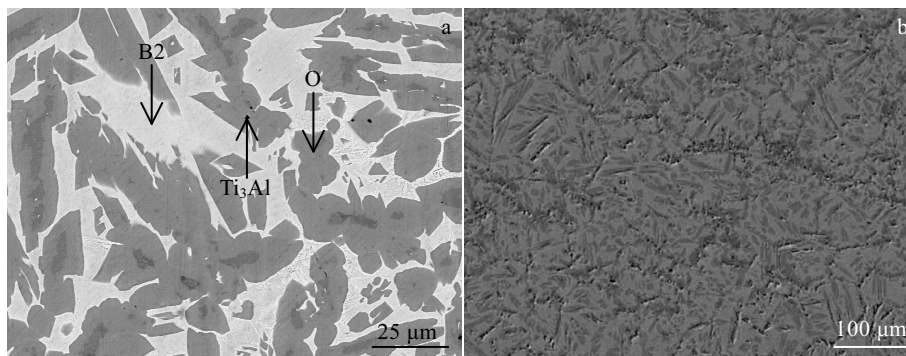
Fig.3   Microstructure of the Ti-22Al-25Nb sintered alloy: (a) BSE image, (b) SE image (the light color marks B2 phases; the grey indicates O phases; the dark grey denotes Ti₃Al phases)

This presented characteristics of the uneven surface with massive particles. This suggested that there was a difference of growth between different phase regions.

Compared with the original microstructure of the sintered alloy in Fig.3, a slight oxidation change was observed, except for few massive particles at 650 °C in Fig. 4a. In particular, no obvious change was observed on the region of O phases (as indicated in Fig. 3). While the temperature rose to 750 °C, the oxidation characteristic of the surface for the sintered alloy became more obvious gradually (especially for B2 phases with a rich-Nb region) which were prone to being oxidized. According to the XRD analyses in Fig. 2, the O phase was still detected. Accordingly, in Fig. 4a and Fig. 4b, the difference of the growth of the oxidation film between O and B2 phases was

still reflected distinctly. This revealed that the O phase had the better oxidation resistance.

When the temperature rose to over 850 °C, the surface oxides grew rapidly. And the difference of the oxidation scales between different phase regions of the sintered alloy was narrowing gradually. This was mainly because the Nb oxides of oxidation scales grew greatly. As described in Fig.1, the stable Nb oxides (Nb_2O_5 or $AlNbO_4$) were dominant when the temperature was above 850 °C. Ralison et al. [16] also confirmed that a mixed oxidation scale mainly consisted of $AlNbO_4$ and TiO_2 at 750 °C. Additionally, a micro crack was formed on the oxidation scale with the increase of the thickness of the oxidation films. This also aggravated the oxidation corrosion of the sintered alloy.
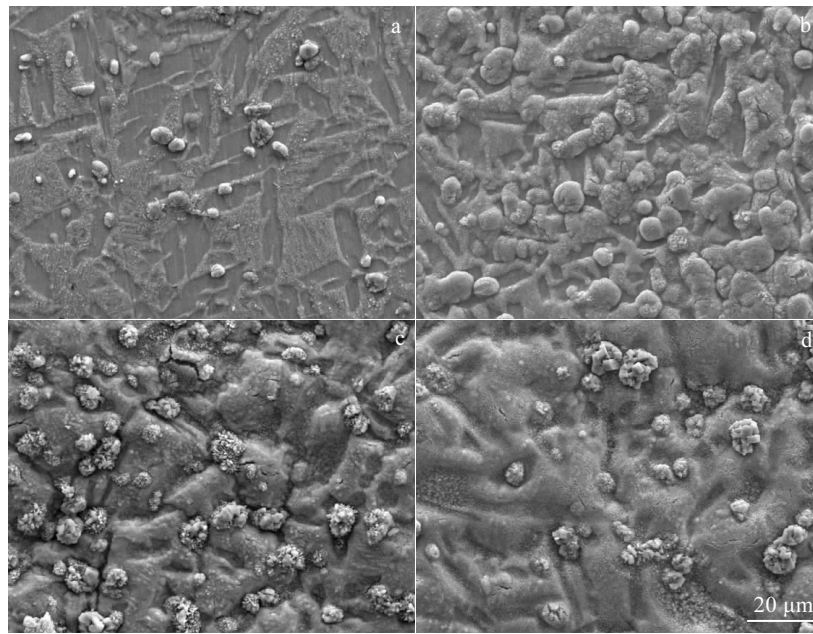
Fig.4   Surface morphologies of samples oxidized for 72 h at 650 °C (a), 750 °C (b), 850 °C (c), 950 °C (d)

Fig.5 shows SEM morphology and EDS analysis of the typical massive particle on the oxidation film. A massive particle was composed of a cluster of small particles, which had a regular shape. This proved that the massive particles were mainly TiO_2, which would be formed on the region of Ti_3Al phases, where there was a poor Nb region. Peng[17] et al. suggested that the activity of Ti, and the saturating and diffusivity of oxygen in Ti_3Al could result in the preferential forming of TiO_2, further promoting the rapid growth of TiO_2 through internal oxidation.

On the other hand, the growth of the oxidation film became faster while the exposure temperature was above 850 °C. The cracks, as a new path of oxygen diffusion, aggravated the oxidation resistance of the sintered alloy. This also explained that the growth rate of oxidation films and mass gains increased evidently. As for the forming mechanism of the cracks on the surface of the oxidation scales, the reason for the formation of the micro cracks could result from internal stress not being released. Meanwhile, the differences of the expansion coefficient and lattice parameters, resulting in mismatching between different phases, could also bring about the crack development.

This was even more apparent when more Nb oxides were formed at higher temperatures. According to the XRD analyses in Fig.1, the metastable Nb_6O continued to be oxidized while the temperature rose above 750 °C. Nb_2O_5 would form and grow and had greater internal stress.

Fig.6 shows the high magnification SEM image of the surface of the oxidation film. As can be seen from Fig. 6, the oxidation film grew rapidly and the oxide on the surface gradually got coarsened with the continuously increased temperature. In addition, at 650 °C, a small amount of grossly coarse particulate oxide and a large amount of fine oxide par-

ticles adhered to the surface of the alloy. As the temperature increased, the oxide particles grew fast with acicular oxides occurring at 750 °C. When the oxidation temperature was raised to 850 °C and 950 °C, the acicular oxide was gradually reduced and the oxide particles were significantly coarsened. The acicular oxide was Al_2O_3, which further reacted with Nb_2O_5 to form the $AlNbO_4$ composite oxide as the oxidation temperature increased. Therefore, the amount of acicular Al_2O_3 was gradually reduced.

Fig.7 shows the results of the SEM observation and EDS analysis of the typical oxide backscattering on the surface of the oxidation film. It can be seen from the backscattering on the oxidation film in Fig. 7 that the surface of the oxidation film was composed of the oxide with coarse granular, the embossed bright color region and the flat gray region. According to the EDS spectrum analysis in Fig. 7a, the granular oxide was chiefly TiO_2, and it can be seen that the particle oxide was mainly formed at the α_2 phase, which was due to the fact that Ti and Al were mixed and oxidized to form TiO_2 and Al_2O_3 mixed oxides when oxidation occurred at the α_2 phase, which lacked the alloying element Nb. TiO_2 grew fast and the growth proceeded with the in-diffusion of oxygen and the out-diffusion of Ti. The preferential formation and rapid growth of the non-protective oxide TiO_2 resulted in the failure of the formation of the continuous dense Al_2O_3 protective oxidation film. In Ref. [18], the X-ray diffraction in-situ observation of the high-temperature oxidation of α_2-Ti_3Al-based alloy showed that TiO_2 was formed first during the high-temperature oxidation of α_2, and Al_2O_3 was formed later and was small in amount, and so the dense Al_2O_3 protective film cannot be formed.
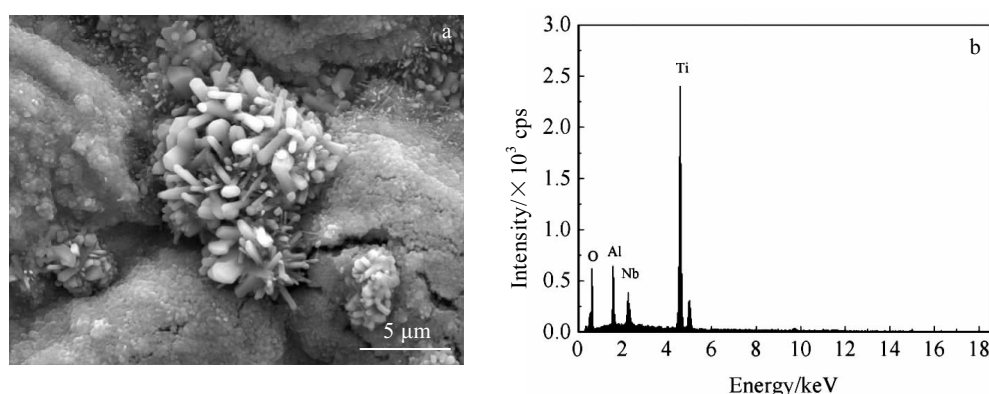
Fig.5　SEM morphology (a) and EDS analysis (b) of the typical massive particle on the oxidation film
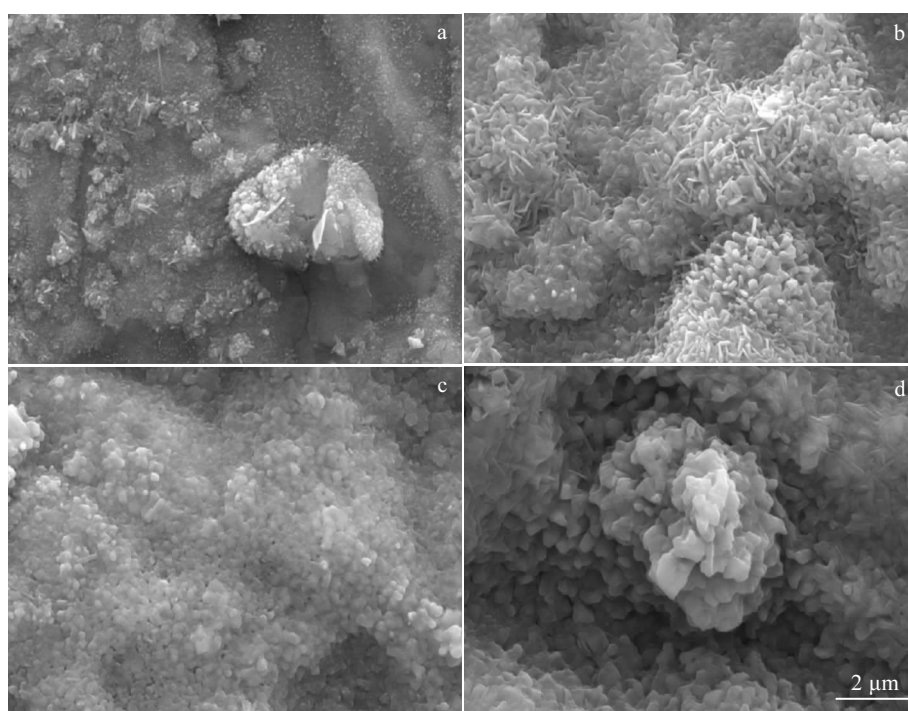
Fig.6　Surface morphologies of samples oxidized for 72 h at 650 °C (a), 750 °C (b), 850 °C (c), and 950 °C (d)

The main Nb-containing phases in the Ti-22Al-25Nb sintered alloy were the B2 phase and O, that is, the O and B2 phase regions. Although the oxidation resistance of B2 phase and O phase were significantly different, in the high temperature oxidation process, the surface of the alloy could form a relatively flat and dense oxide film, which indicated that the presence of the alloy element Nb could improve the morphology of the oxidation film and the oxidation resistance of the alloy. In addition, as can be seen from Fig. 4 and Fig. 7, the Nb-rich region of the oxidation film was prone to cracking, which may be due to the increase in the Nb oxides of Nb_2O_5 or $AlNbO_4$ in the mixed oxide. The growth stress of Nb_2O_5 and $AlNbO_4$ was large, and the stress cannot be released during the process of rapid growth at high temperature, resulting in the cracks on the surface of the oxidation film. As the oxidation temperature increased, the oxidation difference between different phases decreased gradually, especially between the B_2 and O phases. The O phase had significantly better oxidation resistance than the B_2 and α_2 phases in the sintered alloy Ti-22Al-25Nb. The results of the XRD analysis in Fig. 2 verified the formation rules of the oxidation film.

2.3 Cross-sectional morphology observation of oxide films

Fig.8 shows the cross-sectional morphologies of the samples oxidized for 72 h at different temperatures. It was observed in Fig.5 that the thickness of the oxidation scales increased obviously with the increase in temperature. Eventually, the oxidation film even peeled off the substrate at 950 °C. In Fig. 8a, a thin oxidation scale of 2~3 μm thickness was formed on the surface of the sintered alloy at 650 °C. It was found that the
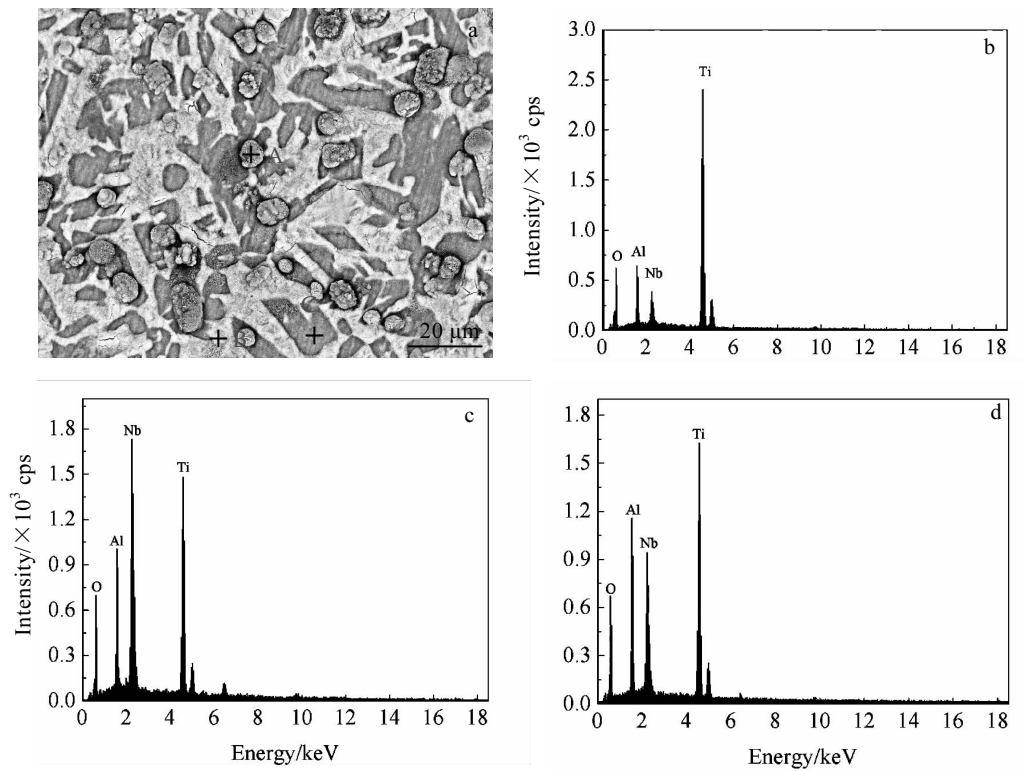
Fig.7   Typical phase composition on the surface of oxidation film: (a) BSE image, (b) EDS analysis of point A, (c) EDS analysis of point B, and (d) EDS analysis of point C

oxidation film was 10~12 μm in thickness, as shown in Fig. 8b. When the exposure temperature rose to over 850 °C, the growth of the oxidation scales became more obvious, and the oxidation scale was 40~50 μm in thickness. The thickness of oxidation film was greater than 100 μm, especially when the exposure temperature was at 950 °C for 72 h. It was apparent that the dense oxidation scale formed on the surface of the sintered alloy below 750 °C.

In addition, as shown in Fig. 8, the dense oxidation scale remained adherent on the substrate below 750 °C. While the exposure temperature was over 850 °C, a loosening of the oxidation scales was formed on the surface of the sintered alloy. In particular, the spallation of oxidation scale was observed on the surface of the sintered alloy when the temperature was at 950 °C, as shown in Fig. 8d.

The reason that the oxidation scale flaked away from the substrate could be the internal stress not being relieved between the oxidation scale and substrate while oxidation scale growing greatly[19]. Thus, the exposure of the new boundary also resulted in further oxidation reaction and mass gain increases, even the occurrence of breakaway oxidation. The integrity of the oxidation scale and substrate was damaged.

2.4   Oxidation kinetics analyses of Ti-22Al-25Nb sintered alloy

The oxidation kinetics curves of Ti-22Al-25Nb sintered alloy were plotted according to the oxidation mass gain (Δm) at different oxidation temperatures, as shown in Fig. 9. The results showed that the oxidation mass gain of the oxidized samples increased with the increase of temperature and holding time. This was consistent with the thickness growth law of oxide film described in Fig. 4 and Fig. 8. At 650 °C, the oxidation mass gain was not obvious, and the alloy exhibited good oxidation resistance.

After a short-term oxidation (less than 24 h), the surface of the oxidized sample had little difference from the initial appearance of the alloy. Even at an oxidation time of 72 h, the maximum oxidation mass gain at 650 °C was only 0.15 mg·cm^{-2}. When the oxidation temperature was 750 °C and 850 °C, the oxidation mass gain of Ti-22Al-25Nb sintered alloy increased rapidly, and the maximum oxidation mass gain of the alloy after oxidation for 72 h was 0.41 and 1.682 mg·cm^{-2}, respectively. As the oxidation temperature increased, the oxidation mass gain became more and more obvious, especially when the temperature rose to 950 °C, and the oxidation mass gain increased sharply. When the oxidation time was more than 48 h, the oxidation mass gain rose steeply, which was totally different from the original oxidation rule, indicating that the oxidation resistance of the sintered alloy Ti-22Al-25Nb deteriorated, which was consistent with the thickness growth rule of the oxidation film shown in Fig. 8. The large amount of non-protective oxide TiO_2 and Nb_2O_5 rose to the failure of the selective oxidation of Al. At the same time, the looseness of
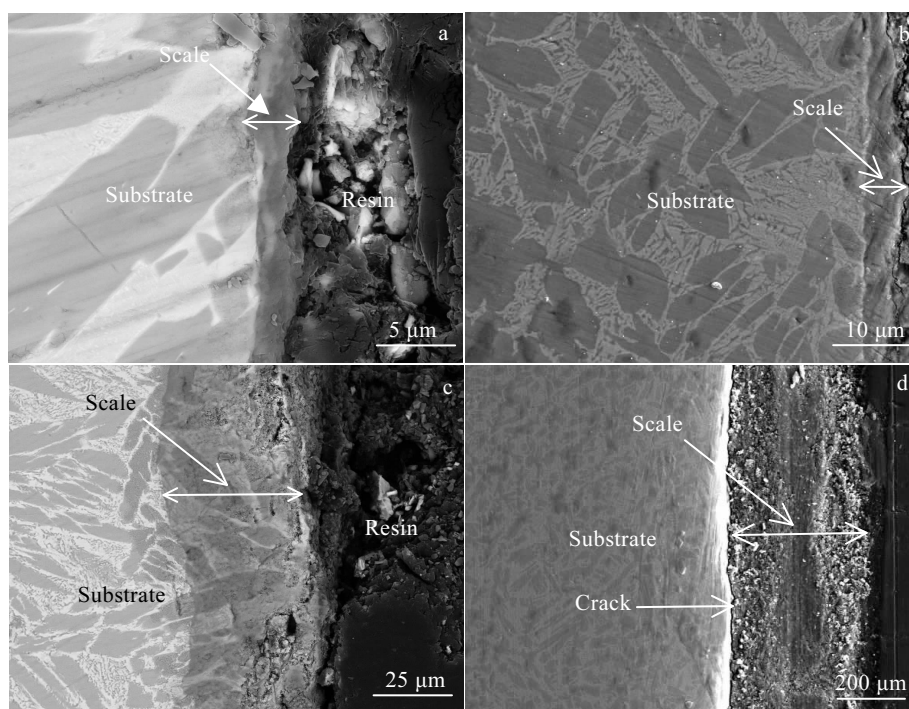
Fig.8   Cross-sectional morphologies of the samples after oxidation for 72 h at 650 °C (a), 750 °C (b), 850 °C (c), and 950 °C (d)

TiO_2 and cracks on the oxidized surface facilitated the rapid diffusion of O_2, which led to the deterioration of the oxidation resistance of the alloy.

At 650 °C and 750 °C, the maximum oxidation mass gains of the sintered alloy Ti-22Al-25Nb after it was heated for 72 h were 0.15 and 0.41 mg·cm^{-2}, respectively. When the oxidation temperature was 850 °C, the maximum oxidation mass gain was 1.682 mg·cm^{-2}. When the oxidation temperature was raised to 950 °C, the oxidation resistance of the alloy deteriorated sharply. Not only was the oxidation mass gain suddenly increased, but also the oxidation film was peeled off. The oxidation mass gain reached 6.9 mg·cm^{-2} after it was heated for 72 h, and its oxidation resistance was in the weak antioxidant range. Table 1 shows the oxidation mass gains of Ti-22Al-25Nb sintered alloy under different oxidation conditions.

Fig.10 describes the oxidation kinetics curves of the Ti-22Al-25Nb sintered alloy at 650, 750, 850 and 950 °C. It can be seen that the oxidation mass gains increased while the temperature rose and holding time increased. This was in accordance with the growth of oxidation scales described in Fig. 3 and 5. The maximum mass gain of the oxidized samples when holding for 72 h at different temperatures (650, 750, 850, 950 °C) were 0.15, 0.41, 1.682 and 6.9 mg·cm^{-2}, respectively.

As mentioned above, the mixed oxides were mainly composed of non-protective TiO_2 and Nb_2O_5, especially when the formation of $AlNbO_4$ oxide resulted in the decreasing of Al_2O_3. The mixed oxide layer could not be effective to improve the oxidation resistance of the sintered alloy due to the loose and
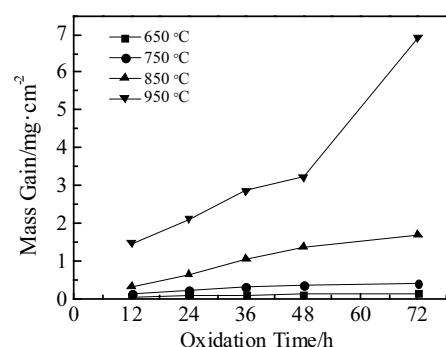
Fig.9   Oxidation kinetics curves of sintered Ti-22Al-25Nb alloy at different temperature

Table 1   Mass gain of reactive sintering Ti-22Al-25Nb alloy for different oxidation time at different temperatures

Oxidation time/h	Mass gain/mg·cm^{-2}			
	650 °C	750 °C	850 °C	950 °C
12	0.059	0.15	0.331	1.48
24	0.085	0.23	0.634	2.12
36	0.10	0.30	1.057	2.853
48	0.12	0.35	1.377	3.242
72	0.15	0.41	1.682	6.9

discontinuous structure. It was generally believed that the oxidation resistance of the alloy decreased because of no presence of continuous Al_2O_3 protective film formed on the

surface of the oxidized sample. In this research, there was not enough Al to achieve the formation of Al_2O_3 protective scale in the Ti-22Al-25Nb sintered alloy due to the lack of preferential oxidation of Al. Yang et al. [20] confirmed that the Al_2O_3 protective scale was formed on the surface of the $TiAl_3$ alloy, which had a higher Al content. The Al_2O_3 scale was formed by means of outward diffusion of Al element. Moreover, Al_2O_3 was further consumed by reacting with Nb_2O_5.

Judging the results of oxidation mass gains according to the standard of HB5258-2000 (aviation industry standard of the People's Republic of China), the oxidation resistance of the Ti-22Al-25Nb sintered alloy met a full anti-oxidation level below 750 °C for 72 h. Even if at 850 °C, its oxidation resistance still achieved an anti-oxidation level. However, there was an occurrence of overall spallation of oxidation film while the oxidation temperature rose up to 950 °C, leading to a deterioration in oxidation resistance. In addition, the mass gains increased sharply.

According to Wagner's high temperature oxidation theory[21], the relation of oxidation mass gain and oxidation time was as follows:

$$\Delta m^n = K_p t \tag{1}$$

where Δm represents the mass gain per unit area (mg·cm^{-2}), n is an oxidation rate exponent, K_p is an oxidation rate constant, and t is the time of exposure. Then, according to the oxidation experimental data of mass gain versus oxidation time, the oxidation rate exponent n and oxidation rate constant K_p were calculated by means of linear regression according to the experimental data of $\ln(\Delta m)$ vs. $\ln t$. The results are listed in Table 2.

Table 2 gives the oxidation rate exponent n and oxidation rate constant of the Ti-22Al-25Nb sintered alloy in the range of 650 to 950 °C. Judged by the experimental results given in Table 1, as the temperatures were at 650 and 750 °C, the oxidation kinetics curves of the samples followed the parabolic law approximately. However, the oxidation curve of the oxidized samples followed the linear law while the oxidation temperature rose to 850 and 950 °C.

The oxidation kinetics exponent changed from parabolic law to linear law with the increasing temperature. Below 750 °C, the oxidation kinetics of the Ti-22Al-25Nb sintered alloy probably followed the parabolic law, which proved that oxidation scales could be effective to resist oxidation behavior. During the lower temperature stage, the oxidation behavior was controlled by atom diffusion. Under the course of oxidation, the parabolic rate constant would depend on the atom diffusion coefficient. However, while the oxidation temperature rose to 850 °C, the oxidation kinetics agreed with the linear law approximately, indicating that the oxidation scales would not provide an effective protection for the sintered alloy, and the oxidation behavior would depend mainly on reaction rate.

From the results in Table 2, at 650 and 750 °C, the parabolic rate constants were 3.46×10^{-4} and 3.03×10^{-3} mg^2·cm^{-4}·h^{-1}, respectively. When the oxidation testing was conducted at 850 °C, the oxidation rate constant was 2.73×10^{-2} mg^2·cm^{-4}·h^{-1}. While the exposure temperature rose to 950 °C, the oxidation rate constant was 2.35×10^{-1} mg^2·cm^{-4}·h^{-1}. While the exposure temperature increased, atomic diffusion coefficient increased, and the oxidation rate went up rapidly. The oxidation rate constant K_p varied from 3.46×10^{-4} to 2.35×10^{-1} mg^2·cm^{-4}·h^{-1} with the temperature ranging from 650 °C to 950 °C, and its variation exceeding 1000 times.

To sum up, the experimental results indicated that the oxidation rate was accelerated as oxidation temperature increased. On the other hand, the oxidation resistance of the sintered alloy decreased gradually with the rising oxidation temperature in the temperature range of 650 to 950 °C. In addition, this also showed that oxidation temperature had a key effect on oxidation rate which could be seen from the data of the oxidation rate constant at different temperatures.

2.5　Oxidation mechanism of the Ti-22Al-25Nb sintered alloy at high temperature

Zhao et al. [22] found that Nb addition would change the oxidation kinetics law of the Ti-Al system. They also pointed out that the oxidation kinetics law would make the transition from the linear law to the parabolic law due to the act of Nb addition. They also stated that Nb addition could improve the oxidation behavior of the TiAl alloy.

All of the TiO_2, Al_2O_3, Nb_2O_5 were n-type semiconductor oxides, which had excessive metal ions in their oxides. According to thermal analysis, Al could be oxidized to form the protective scale of Al_2O_3 in preference to Ti transforming into TiO_2 in theory. Meanwhile, it was necessary to have enough Al to make Al_2O_3 to form a continuous and dense protective scale. However, the diffusivity of Ti^{4+} was faster than that of Al^{3+} in Ti-Al alloy. Thus, depending on the kinetics factors, TiO_2 was formed in preference to Al_2O_3 in the Ti-22Al-25Nb sintered alloy. In addition, Nb^{5+} in Nb_2O_5 could provide more free electrons to decrease the point defects relative to Ti^{4+} and Al^{3+}, and further to inhibit internal oxidation. Additionally, Nb could inhibit the formation and growth of TiO_2 owing to the enhancement of the activity of Al and the inhibited oxidation of Ti [23]. That is, Nb addition not only inhibited the diffusion of Ti and oxygen ions, but also improved the structure and morphologies of the oxidation scale[24]. The discontinuous oxidation scale could result from the formation of TiO_2 and Al_2O_3 competitively. In addition, the discontinuous unprotected Al_2O_3 could also be caused by low Al content and high Nb content.

As mentioned above in Fig.4, a cluster of TiO_2 was produced owing to the lack of Nb additive; however, excessive Nb additive would also result in the deterioration of the oxidation resistance of the sintered alloy owing to the formation of redundant Nb oxide. Based on the analyses of phase identifica-
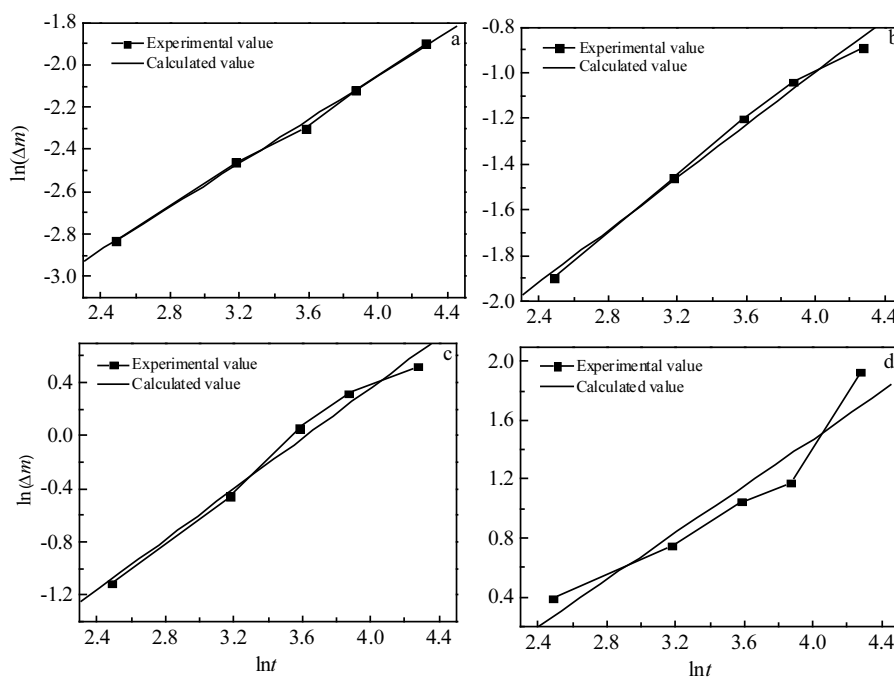
Fig.10 Oxidation kinetics curves of Ti-22Al-25Nb sintered alloy at 650 °C (a), 750 °C (b), 850 °C (c), and 950 °C (d)

Table 2 Exponent *n* and oxidation rate constant K_p of the Ti-22Al-25Nb sintered alloy in the range of 650~950 °C

Oxidation temperature/°C	n	K_p/mg^2·cm^{-4}·h^{-1}
650	1.95	3.46×10^{-4}
750	1.76	3.03×10^{-3}
850	1.05	2.73×10^{-2}
950	1.23	2.35×10^{-1}

tion in Fig. 1 and the morphology observations in Fig. 3, it was found that oxides developed slower on the surface of O phases compared to Ti₃Al and B2 phases below 750 °C. In this research, it was also proved that the oxidation resistance of a B2 field with higher Nb content or a Ti₃Al phase with lower Nb content was not as good as that of the O phase. This proved that too little or excessive Nb additive would result in the oxidation resistance deteriorating. Oxidation kinetics curves varied with the oxidation mechanism. M. Mitoraj et al. [25] confirmed that the inward diffusion of oxygen would play a predominant role on the oxidation resistance. So, the sharp decreasing of oxidation resistance would result from internal oxidation occurring while the inward diffusion of oxygen surpassed the outward diffusion of metal cation.

The grain boundary, as a short-circuit diffusion path because of a high defect-density, resulted in the significant difference of activation energy between the grain boundary diffusion and bulk diffusion. Its positive effect would facilitate selective oxidation, but the preferential oxidation of Al in the Ti-22Al-25Nb sintered alloy was owing to the lower Al content,

which was not enough to promote the formation of a protective oxidation scale of Al₂O₃. On the contrary, a negative effect of the grain boundary that resulted from the increasing of grain boundaries area would affect the oxidation resistance of the sintered alloy. Therefore, the Ti-22Al-25Nb sintered alloy with large grains just obtained good oxidation resistance, which resulted from avoiding a large number of grain boundaries to provide more diffusion paths. Additionally, defects, such as pores, which were defined as diffusion porosity according to the Kirkendall effect, could form due to Al diffusion. The Ti-22Al-25Nb sintered alloy prepared by powder metallurgy could generate redundant pores in the sintered alloy intrinsically. All of these could facilitate the inward diffusion of oxygen, further deteriorating the oxidation resistance of the sintered alloy.

3 Conclusions

1) The oxidation mass gain of Ti-22Al-25Nb was obtained at different temperatures. The maximum mass gains were obtained as follows: 0.15, 0.41, 1.682 and 6.9 mg·cm⁻² at 650, 750, 850 and 950 °C, respectively. Judged by the results, the Ti-22Al-25Nb sintered alloy met a full anti-oxidation resistance level below 750 °C. Even if the temperature rose to 850 °C, it was still up to anti-oxidation level.

2) The oxidation kinetics approximately followed the parabolic law when the oxidation temperature was below 750 °C. However, while the exposure temperature rose above 850 °C, the linear law was fitted. The parabolic rate

constants at 650 and 750 °C were 3.46×10^{-4} and 3.03×10^{-3} $mg^2 \cdot cm^{-4} \cdot h^{-1}$, respectively. At 850 and 950 °C, the oxidation rate constants were 2.73×10^{-2} and 2.35×10^{-1} $mg^2 \cdot cm^{-4} \cdot h^{-1}$, respectively.

3) The mixed oxide scale mainly consisted of TiO_2 and $AlNbO_4$, especially at a higher exposure temperature. The Ti-22Al-25Nb sintered alloy exhibited good oxidation resistance below 850 °C, and oxidation scales still remained adherent on the matrix. However, at 950 °C, the oxidation resistance deteriorated sharply, and the oxidation scale even peeled off the matrix of the Ti-22Al-25Nb sintered alloy.

4) In the Ti-22Al-25Nb sintered alloy, the O phase exhibited better oxidation resistance than rich-NbB_2 and lean-Nb Ti_3Al phases. This also proved that too little or excessive Nb additive would result in the oxidation resistance deteriorating. In addition, the oxidation mechanism could explain the fact that Nb additive did not only inhibit the diffusion of metal ions and oxygen, but also improved the structure and morphologies of oxidation scale.

References

1 Lin P, Hao Y G, Zhang B Y *et al. Materials Science and Engineering A*[J], 2018, 710: 336

2 PintK B A, MoreI L, Wright G. *Oxidation of Metals*[J], 2003, 59: 257

3 Polozov I, Sufiiarov V, Popovich A *et al. Journal of Alloys and Compounds*[J], 2018, 763: 436

4 Yang Y, Kitashima T, Hara T *et al. Oxidation of Metals*[J], 2017, 88: 583

5 Hadi M, Bayat O, Meratian M *et al. Oxidation of Metals*[J], 2018, 90: 421

6 Banerjee D, Gogia A K, Nandy T K *et al. Acta Metallurgica*[J], 1988, 36: 871

7 Wei F, Se-Hyun K, Hitoshi H *et al. Materials Science and Engineering A*[J], 2002, 329-331: 708

8 Cai D T, Chen J C, Mao X F *et al. Intermetallics*[J], 2013, 38: 63

9 Li Y J, Zhao Y, Li Q *et al. Materials & Design*[J], 2017, 114: 226

10 He L J, Su H H, Xu J H *et al. The International Journal of Advanced Manufacturing Technology*[J], 2017, 92: 4415

11 Zhang Q C, Chen M H, Wang H *et al. Transactions of Nonferrous Metals Society of China*[J], 2016, 26: 722

12 Wu H Y, Zhang P Z, Zhao H F *et al. Applied Surface Science*[J], 2011, 257: 1835

13 Chen X, Xie F, Ma T *et al. Advanced Engineering Materials*[J], 2016, 18: 1944

14 Leyens C. *Oxidation of Metals*[J], 1999, 52: 475

15 Li H Q, Wang Q M, Gong J *et al. Applied Surface Science*[J], 2011, 257: 4105

16 Ralison A, Dettenwanger F, Schütze M. *Materials and Corrosion*[J], 2000, 51: 317

17 Peng X M, Xia C Q, Wang Z H *et al. The Chinese Journal of Nonferrous Metals*[J], 2010, 20: 1116

18 Zhang L T, Wu J S. *Rare Metal Materials and Engineering*[J], 1997, 26(2): 23 (in Chinese)

19 Zhang Z G, Wang Y J, Xiao L J *et al. Corrosion Science*[J], 2012, 64: 137

20 Yang W S, Xiu Z Y, Wang X *et al. Materials & Design*, 2011, 32: 207

21 Li Tiefan. *High Temperature Oxidation and Hot Corrosion of Metals* [M]. Beijing: Chemical Industry Press, 2004: 35 (in Chinese)

22 Zhao L L, Lin J P, Wang Y L *et al. Acta Metallurgica Sinica*[J], 2008, 44: 557

23 Li Y F, Xu H, Song Z Q *et al. Journal of Central South University of Technology*[J], 2010, 17: 674

24 Leyens C, Schmidt M, Peters M *et al. Materials Science and Engineering A*[J], 1997, 239: 680

25 Mitoraj M, Godlewska E, Heintz O *et al. Intermetallics*[J], 2011, 19: 39

反应烧结 Ti-22Al-25Nb 合金的高温氧化行为

王长瑞 [1,3]，王远鑫 [2]，张凯锋 [2]

(1. 南京航空航天大学，江苏 南京 210016)
(2. 哈尔滨工业大学，黑龙江 哈尔滨 150001)
(3. 中国电子科技有限公司 第十四研究所，江苏 南京 210039)

摘 要：Ti-22Al-25Nb 是一种高温结构材料，它的抗氧化性对今后的发展和应用具有重要意义。采用元素粉末和反应烧结法制备了 Ti-22Al-25Nb 烧结合金，研究了其在静态空气中的氧化行为 (923~950 °C 温度范围内)。不同温度 (650, 750, 850, 950 °C)下的最大增重分别为 0.15, 0.41, 1.68 和 6.9 $mg \cdot cm^{-2}$。研究发现 Ti-22Al-25Nb 烧结合金具有良好的抗氧化性，特别是在 750 °C 以下 (950 °C 时发生氧化分解)。根据氧化动力学分析，在 750 °C 以下，氧化行为大致遵循抛物线规律，而在 850 °C 以上，氧化行为符合线性规律。讨论了铌合金元素对氧化动力学的影响，通过对氧化形态和相的观察和分析，证明 O 相（有序 Ti_2AlNb 相）的抗氧化性能优于其它相，其原因可以解释为不同相的 Nb 含量的差异导致抗氧化性的差异。

关键词：Ti-22Al-25Nb烧结合金；有序晶相；高温氧化；氧化机理

作者简介：王长瑞，男，1983 年生，博士，中国电子科技有限公司第十四研究所，江苏 南京 210039, E-mail: wchrui2016@163.com